Biological Journal of the Linnean Society, 2019, **XX**, 1–19. With 5 figures.

Multiple components of feather microstructure contribute to structural plumage colour diversity in fairy-wrens

MARIE FAN[1,*], LILIANA D'ALBA[2], MATTHEW D. SHAWKEY[2], ANNE PETERS[1] and KASPAR DELHEY[1,3]

[1]*School of Biological Sciences, Monash University, 25 Rainforest Walk, Clayton, Victoria 3800, Australia*
[2]*Evolution and Optics of Nanostructures Group, Department of Biology, University of Ghent, Ledeganckstraat 35, Ghent 9000, Belgium*
[3]*Max Planck Institute for Ornithology, Vogelwarte Radolfzell, Am Obstberg 1, D-83175, Radolfzell, Germany*

Received 21 March 2019; revised 1 July 2019; accepted for publication 1 July 2019

Closely related species often differ in coloration. Understanding the mechanistic bases of such differences can reveal whether evolutionary changes in colour are driven by single key mechanisms or changes in multiple pathways. Non-iridescent structural plumage colours in birds are a good model in which to test these questions. These colours result from light absorption by pigments, light scattering by the medullary spongy layer (a nanostructure found within barbs) and contributions from other structural elements. Fairy-wrens (*Malurus* spp.) are a small clade of closely related birds that display a large diversity of ornamental structural colours. Using spectrometry, electron microscopy and Fourier analysis, we show that 30 structural colours, varying from ultraviolet to blue and purple, share a similar barb morphology. Despite this similarity, we find that at the microscopic scale, variation across multiple structural elements, including the size and density of the keratin cortex, spongy layer and melanin, explains colour diversity. These independent axes of morphological variation together account for sizeable amounts of structural colour variability (R^2 = 0.21–0.65). The coexistence of many independent, evolutionarily labile mechanisms that generate colour variation suggests that the diversity of structural colours in this clade could be mediated by many independent genetic and environmental factors.

ADDITIONAL KEYWORDS: avian visual space – colour evolution – feather nanostructure – Fourier analysis – *Malurus* – ornamental plumage.

INTRODUCTION

Ornamental coloration features prominently in animal communication, sexual selection and speciation (Darwin, 1871; Andersson, 1994). In many animal clades, closely related species differ considerably in the colours they display, and understanding the mechanistic changes behind these differences can provide insights into the evolution of colour divergence. Bird plumages constitute some of the most diverse colour displays and have served as a classic model system to study the evolution of ornaments (Hill & McGraw, 2006). Feather coloration can be produced by two main mechanisms: the deposition of pigments (e.g. melanins and carotenoids) that selectively absorb some wavelengths of light while allowing others to be reflected (McGraw, 2006), or the physical interaction between light and biological tissues that vary periodically in refractive index at the nanometre scale (i.e. structural coloration; Prum, 2006). Structural colours include most blue, violet and ultraviolet (UV) hues and iridescent colours (Prum, 2006). Although these two mechanisms are often studied in isolation, many colours are created by the interactions of pigmentary and structural components, and variations in either mechanism can cause changes in the resulting coloration (Shawkey & Hill, 2005,

*Corresponding author. E-mail: mary.f18@gmail.com

2006; Prum, 2006; Driskell *et al.*, 2010; Shawkey & Alba, 2017).

Structural colours are inherently linked to the nanostructural characteristics of the underlying morphology. Non-iridescent blue, violet and UV colours primarily result from arrays of keratin and air within feather barbs that form the medullary 'spongy layer' (Prum, 2006; Prum *et al.*, 2009; Saranathan *et al.*, 2012). Many studies on such colours have therefore focused on the role of the spongy layer, which constitutes the main colour-producing element in the barb (Prum, 2006). Nevertheless, the morphology of the feather barb is complex, with many other structural elements that may vary and interact with the spongy layer. To date, how this morphological complexity generates interspecific colour variation, through changes in many structural elements, has rarely been investigated in non-iridescent structural colours (for an example for iridescent structural colours that are produced by arrays of melanin granules, see Eliason *et al.*, 2015). As far as we know, only one study has established a link between non-iridescent UV–blue coloration and the keratin cortex (Shawkey *et al.*, 2005). Moreover, although the presence of melanin beneath the spongy layer is essential, because it absorbs incoherently scattered white light that would otherwise wash out the coherently scattered colour (Prum, 2006; Shawkey & Hill, 2006; Shawkey & Alba, 2017), whether its arrangement (organization, spacing) or density affects non-iridescent structural coloration remains unclear.

Male fairy-wrens in the genus *Malurus* display a great variety of brightly coloured plumages, often rich in short-wavelength reflectance, including blue, indigo and almost pure UV hues (Fig. 1). Most of these colourful plumages are seasonal (nuptial), and in several species they serve sexually selected functions, through female choice or male–male competition (Cockburn *et al.*, 2008; Peters *et al.*, 2013; Fan *et al.*, 2018). Although studies have confirmed the contribution of the medullary spongy layer to the production of structural colours in fairy-wrens (Doucet *et al.*, 2004; Driskell *et al.*, 2010; Saranathan *et al.*, 2012), the contribution of the different aspects of feather morphological variation to explaining colour

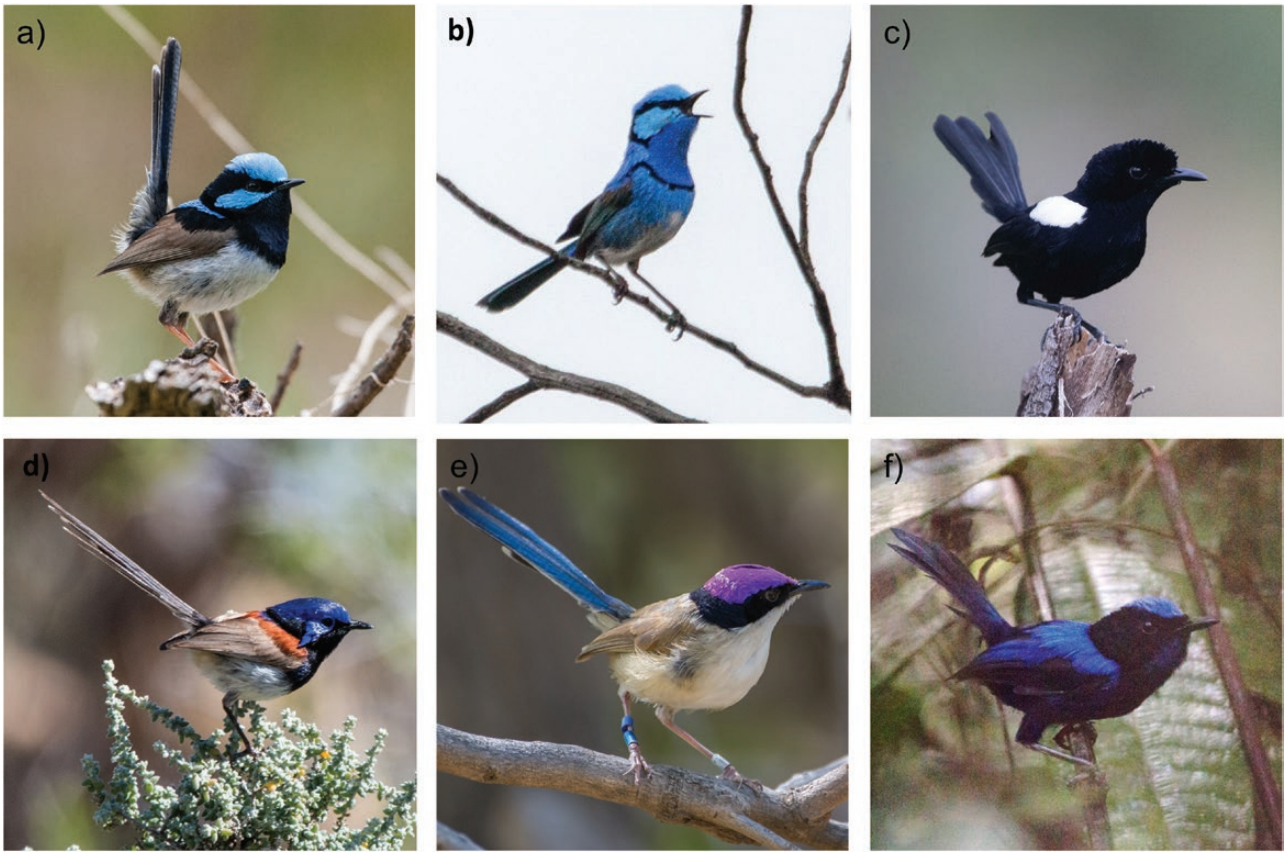

Figure 1. Male fairy-wrens (*Malurus* spp.) display a great diversity of nuptial plumages, including various structural colours. Shown are photographs of a male *M. cyaneus* (A), *M. splendens* (B), *M. alboscapulatus* (C), *M. lamberti* (D), *M. coronatus* (E) and *M. cyanocephalus* (F), in nuptial plumage. Photographs: A, B, D, K. Delhey; C, F, E. Enbody; and E, L. Lermusiaux.

diversity has not been assessed. Here, we investigate the mechanistic causes of the variability in structural plumage coloration in this genus to identify the key aspects of morphological variation that underpin it.

MATERIAL AND METHODS

Study species

To investigate how feather barb structure influences the expression of structural colours, we selected all nine species of *Malurus* in which males display structural colours, i.e. blue, indigo and purple plumage patches (*Malurus cyanocephalus*, *Malurus coronatus*, *Malurus elegans*, *Malurus pulcherrimus*, *Malurus amabilis*, *Malurus lamberti*, *Malurus cyaneus*, *Malurus splendens* and *Malurus leucopterus*; Supporting Information, Fig. S1). Some species included multiple subspecies with varying structural colours, and in those cases we included samples for the different subspecies. For each taxon, we sampled between one and five differently coloured structural plumage patches (full details are provided in Supporting Information, Appendix S1; Table S1). Feathers were pulled from living birds and museum specimens using tweezers and stored in small manila envelopes at ambient temperature until the time of analysis. Hereafter, we use the term 'unique patch' to refer to a single plumage patch of a given taxon (e.g. the blue throat of *Malurus splendens splendens*).

In addition, we compared these structurally coloured plumages with two other nuptial colours displayed in the genus, black and rufous, by examining the barb structure of rufous feathers from *M. elegans*, *M. pulcherrimus*, *M. amabilis* and *M. lamberti*, and black feathers from *M. coronatus*, *M. lamberti* and *M. splendens*, in addition to *Malurus alboscapulatus* and *Malurus melanocephalus* (Supporting Information, Fig. S1). These black and rufous feathers were sampled only to describe their microstructure, because previous work revealed that black plumage in other fairy-wren species presented microstructural elements consistent with structural UV/blue colours whose contribution had been obliterated by high melanin deposition (Doucet *et al.*, 2004; Driskell *et al.*, 2010).

Reflectance spectrometry and visual models

The reflectance of each unique patch was measured on museum specimens and living birds (N = 8–717 for each patch; for details see Supporting Information, Table S2; average spectra in Supporting Information, Figs S2, S3) using an AvaSpec-2048 spectrometer connected to an AvaLight-XE xenon pulsed light source (Avantes) with a bifurcated fibre-optic cable fitted at the end with a cylindrical plastic probe (6 mm diameter) to standardize measuring distance (5 mm) and angle (90°) and exclude ambient light. We held the probe perpendicular to the surface of the plumage, and collected up to five reflectance spectra per plumage patch. Reflectance between 300 and 700 nm was calculated relative to a WS-2 white standard using the software AVASOFT v.7.5 (Avantes; Fig. 2; Supporting Information, Figs S2, S3).

To summarize spectral information, we used psychophysical models of avian colour vision (Vorobyev *et al.*, 1998), following the methods described by Delhey *et al.* (2015). The main advantage of using visual models is that, unlike other descriptors of spectral shape variation, which are often tailored to a specific type of reflectance spectrum, their output can be directly compared across different types of colours (see further discussion by Delhey & Peters, 2008; Delhey *et al.*, 2015). Moreover, the second advantage is that visual models bring us closer to the perceptual world of receivers, hence they can provide information on the putative biological relevance of colour differences. However, this also constitutes their main weakness, because often we do not have detailed information on all required visual parameters for our study species, and we need to use information from other species.

Visual models require knowledge of the visual sensitivity functions of the four types of cones used by birds in colour vision, the relative abundance of each of these cones in the retina and the spectrum of illuminating light. Colour vision in birds is mediated by four types of single cones sensitive to very short (VS), short (S), medium (M) and long (L) wavelengths of light (Vorobyev *et al.*, 1998). Variation in visual sensitivity between species is mainly restricted to the VS and S cones, and birds can generally be classified into two groups: ultraviolet-sensitive (U-type) and violet-sensitive (V-type) species, where U-type species have VS cones with the peak sensitivity shifted towards shorter wavelengths (Hart & Hunt, 2007). Fairy-wrens are unique in that within the genus *Malurus* there are species with V-type and species with U-type visual sensitivities (Odeen *et al.*, 2012). Therefore, we modelled both sensitivity types to see whether it affected the results (Bitton *et al.*, 2017) (visual sensitivity functions obtained from Endler & Mielke, 2005).

Visual models also require knowledge of the noise-to-signal ratios for each of the four different cone types, which can be approximated by knowing the relative amounts of each cone type in the retina. Given that the relative abundance of the four cones in the retina does not differ consistently between U- and V-type species (Hart, 2001), and we have no data for any *Malurus* species, we used average cone proportions computed from Hart (2001) (0.38:0.69:1.14:1.00 for

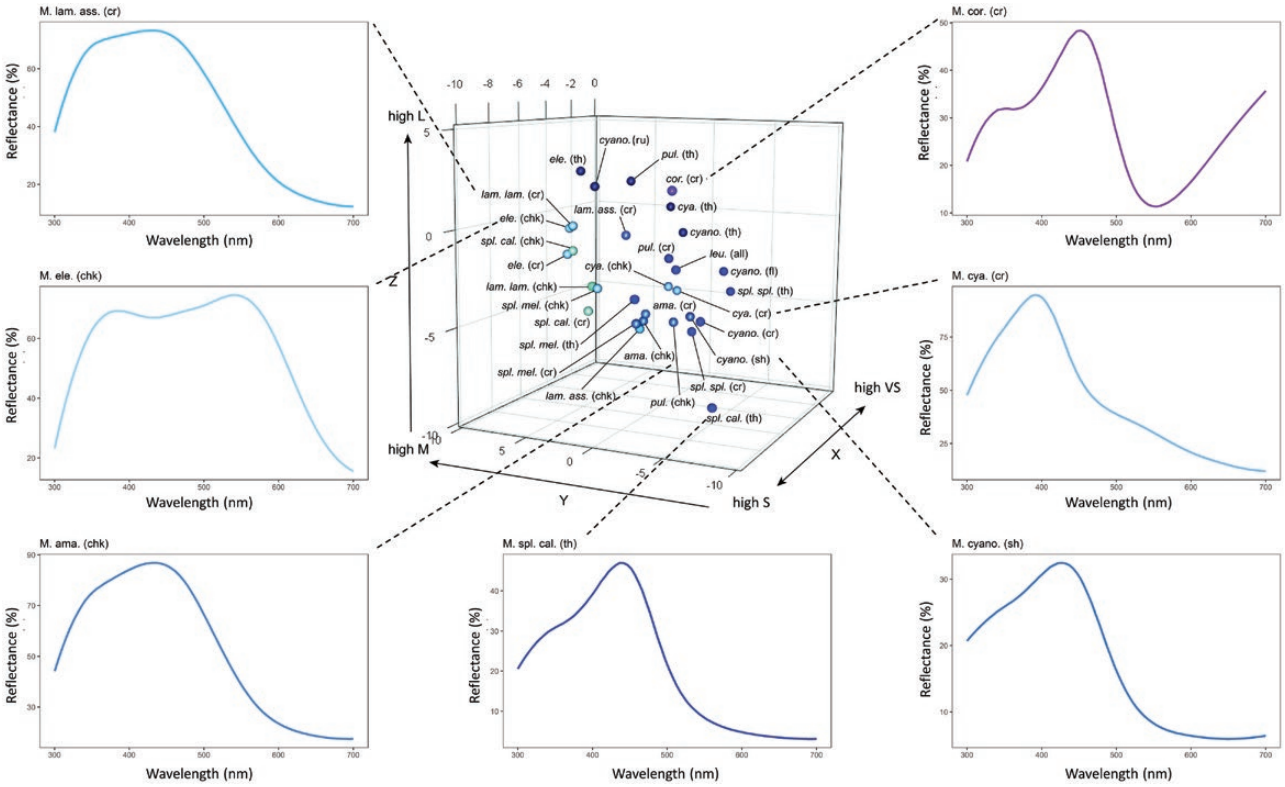

Figure 2. Linking reflectance spectra with chromatic coordinates. The central panel depicts the positions of the studied structurally coloured patches in the visual space of U-type eyes, where sphere colours correspond approximately to the feather colour perceived by the human eye. The surrounding panels show examples of average (smoothed) plumage reflectance spectra matched with their position in visual space (dotted lines). Taxon abbreviations: *ama.*, *Malurus amabilis*; *cor.*, *Malurus coronatus* (*coronatus*); *cya.*, *Malurus cyaneus* (*cyaneus*); *cyano.*, *Malurus cyanocephalus* (*bonapartii*); *ele.*, *Malurus elegans*; *lam. ass.*, *Malurus lamberti assimilis*; *lam. lam.*, *Malurus lamberti lamberti*; *leu.*, *Malurus leucopterus* (*leuconotus*); *pul.*, *Malurus pulcherrimus*; *spl. cal.*, *Malurus splendens callainus*; *spl. mel.*, *Malurus splendens melanotus*; *spl. spl.*, *Malurus splendens splendens*. Plumage patch abbreviations: all, the whole body except the wings and tail for *M. leucopterus*; ch, cheek; cr, crown; fl, flank, ru, rump; sh, shoulder; th, throat.

VS:S:M:L). Cone proportions were combined with behavioural estimates of the Weber fraction (0.1; Olsson *et al.*, 2017), using formula (10) of Vorobyev *et al.* (1998) to obtain the noise-to-signal ratios (ν) for each cone type (ν_{VS} = 0.162, ν_S = 0.120, ν_M = 0.094, ν_L = 0.1). Although data on relative cone proportions are scarce, in general birds have similar amounts of L and M cones, fewer S cones and even fewer VS cones, and variation is relatively limited (Hart, 2001). This is why systematically running visual models using all known cone proportions generally yields similar results (see supplementary material of Delhey *et al.*, 2013), except for outlier species, such as the little pied cormorant (*Phalacrocorax varius*), with extremely high proportions of VS cones (Hart, 2001). Finally, we used the spectrum of standard daylight (D65, open habitats) as illuminant (Vorobyev *et al.*, 1998). This is representative of the light environment for most species of fairy-wren, which are found in open habitats. Moreover, the choice of irradiance has minimal effects on the outcome of visual models, as shown for fairy-wrens (Delhey *et al.*, 2013) and other species (Delhey & Peters, 2008).

Visual models yield a set of quantum catches for the four types of single cones (i.e. how much each type of cone is stimulated by a specific combination of reflectance spectrum and irradiance) that can be transformed into three coordinates, *x*, *y* and *z*, that define the position of each spectrum in the visual space of birds (Fig. 2; Supporting Information, Fig. S4). This visual space takes the shape of a tetrahedron, where each apex represents the sole stimulation of one cone type (Burkhardt, 1989; Goldsmith, 1990). Using the formulae of Cassey *et al.* (2008), distances between points in visual space are measured in 'just-noticeable differences' (jnd), whereby distances >1 jnd are considered to be discriminable by birds. For each unique structurally coloured patch (i.e. excluding

black and rufous patches), we computed the average position, or centroid, of the patch in the visual space (Fig. 2; Supporting Information, Fig. S4), in addition to the standard error (SE) around each chromatic coordinate (x, y and z). Likewise, for each spectrum we computed achromatic variability (i.e. 'perceived brightness' or luminance variation, measured in just-noticeable differences) based on cone quantum catch of double cones (which mediate perception of achromatic cues in birds; Cuthill, 2006) as described by Delhey *et al.* (2015), using formula (7) of Siddiqi *et al.* (2004) and a noise-to-signal ratio of 0.2 (Olsson *et al.*, 2017), and subsequently, computed the average perceived brightness and SE for each unique patch.

Additionally, to provide a set of spectral shape variables that are independent of visual models and can be compared with results from previous studies, we also computed: (1) hue (the wavelength of peak reflectance) as an index of spectral location; (2) UV chroma (the summed reflectance of light in the range of 300–400 nm divided by the summed reflectance in the range 300–700 nm); (3) spectral saturation (the proportion of light reflected around the reflectance peak with reflectance equal to or larger to half of that of the peak) both as indices of colour purity (Andersson *et al.*, 1998); and (4) brightness (mean reflectance) as an index of achromatic variation, using the package 'pavo' (Maia *et al.*, 2013) in R v.3.4.0 (R Development Core Team, 2014).

Using these variables provides indicators of spectral shape that are free from some of the complexities and uncertainties of visual models, but they also have limitations. The most important one is that they cannot fully capture the complexity of spectral variability. For example, the results for hue and spectral saturation should be interpreted with caution, given that many of the measured spectra display multiple peaks, with substantial variation in the height and location of the primary and secondary peaks (Fig. 2; Supporting Information, Fig. S2). Likewise, UV chroma is a rather arbitrary variable that focuses on a specific part of the spectrum of particular interest owing to its human-invisible nature but that might not be especially important for avian colour signalling (Stevens & Cuthill, 2007).

Transmission electron microscopy

To characterize the feather micro- and nanostructural elements responsible for the colours of the different studied patches, we used transmission electron microscopy (TEM). We prepared samples following a protocol similar to that of Shawkey *et al.* (2003). Briefly, we cut feather barbs from the upper 5 mm of contour feathers, washed them in 100% ethanol (twice, for 20 min each time) and infiltrated them with Epon in successive concentrations of 15, 50, 70 and 100% (24 h each time). Barbs were then placed into moulds and, after curing the blocks at 60 °C for 16 h in an oven, we trimmed them with a Leica S6 EM Trim2 (Leica Microsystems) and cut 100 nm thin sections using a Leica EM UC6 ultramicrotome (Leica Microsystems) equipped with a MT14878 DiATOME diamond knife (DiATOME). Sections were transferred with a loop to copper grids, stained with uranyl acetate and lead citrate and viewed on a Jeol JEM-1010 transmission electronic microscope (Jeol Ltd). Micrographs were taken at magnifications between ×800 and ×30 000 (Fig. 3; Supporting Information, Appendix S2).

Our study focuses on the role of the barb structure; therefore, we did not investigate the role of barbules, which were present only in very dark blue and indigo feathers (N = 6 of 30 structurally coloured feathers), and in black and rufous feathers (Supporting Information, Fig. S3). We measured the reflectance of individual barbs at normal incidence using a Craic AX10 UV–visible microspectrophotometer (Craic Technologies, Inc., San Dimas, CA, USA) with a ×15 glass objective lens, and the spectra were very similar to those of the corresponding plumage patches (Supporting Information, Fig. S5). This suggests that the effect of barbules on the overall plumage colour is probably not affecting our conclusions (for further discussion on the effects of barbules in this genus, see Enbody *et al.*, 2017).

Microstructural variation

We used ImageJ v.1.51 (Schneider *et al.*, 2012) to measure the thickness of the keratin cortex and spongy layer (the latter for structurally coloured patches only, because black and rufous barbs have little, degraded or no spongy layer; Fig. 3F, G) at six different evenly spaced points around the barb. Given that black and rufous feathers have a pointed shape (and not an oval or round shape), we avoided the pointed area to measure the cortex thickness. Using both ImageJ v.1.51 and MATLAB, we also measured the cross-sectional area of the spongy layer and of the melanin granules underneath to estimate the ratio of melanin to spongy layer (for structurally coloured patches only). These parameters may affect the amount and/or range of wavelengths of light absorbed by the barb (Shawkey *et al.*, 2006; Shawkey & Hill, 2006; D'Alba *et al.*, 2012) and therefore the reflected colour.

Fourier analysis

For all structurally coloured patches, we performed a two-dimensional Fourier analysis on TEM images of feather barbs using the two-dimensional fast Fourier transform tool of ImageJ v.1.51. This analysis allows us

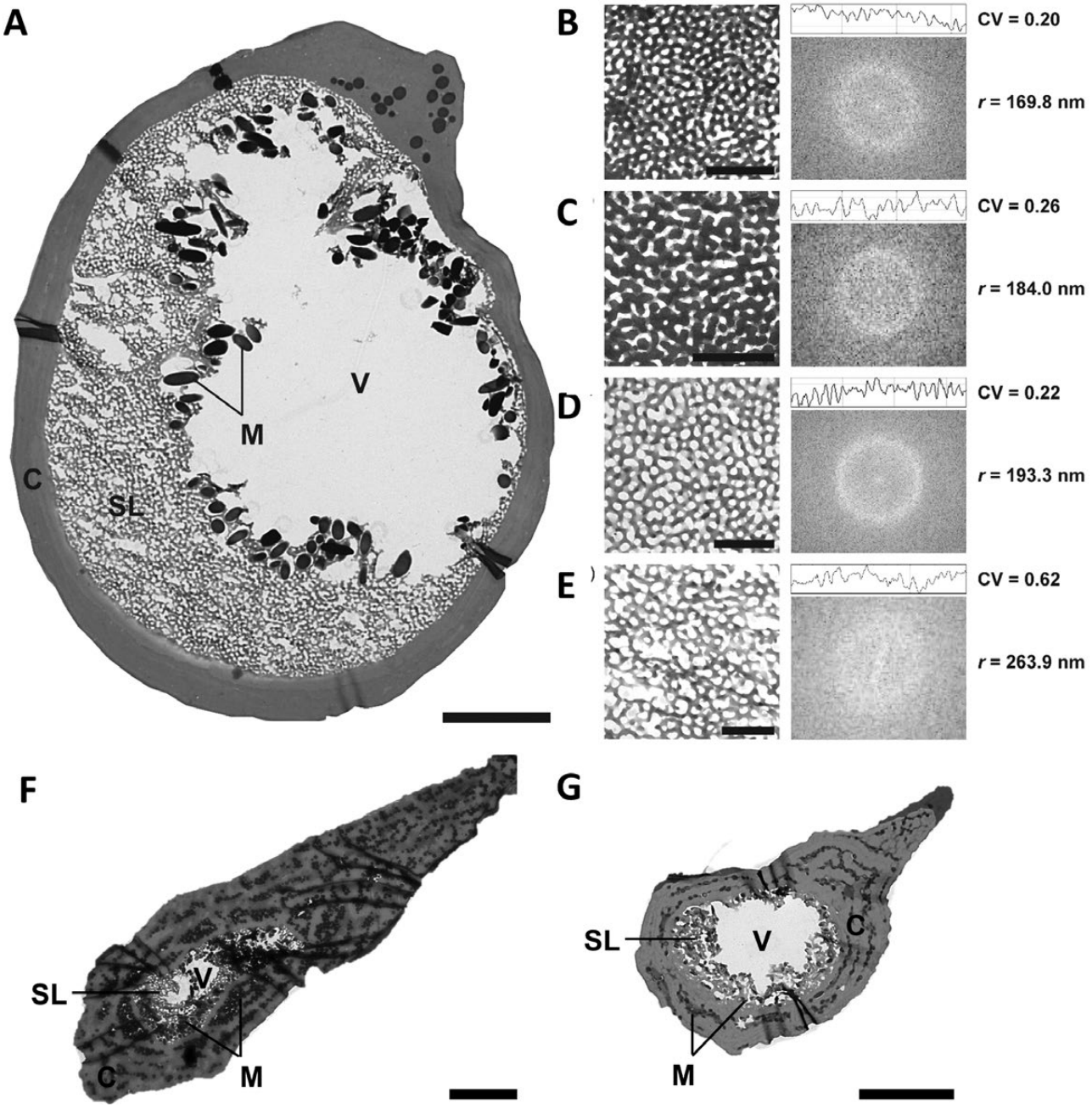

Figure 3. A, feather barb microstructure from a structurally coloured plumage patch. Shown is a transmission electron microscopy (TEM) image of a cross-section of a feather barb collected from the blue crown of a male *Malurus elegans*. Scale bar: 5 μm. B–E, spongy layer characteristics. Shown are TEM images of the spongy layer found in the feather barbs collected from the throat of a male *Malurus cyaneus cyaneus* (B), the crown of a male *Malurus coronatus coronatus* (C), the throat of a male *Malurus splendens melanotus* (D) and the crown of a male *Malurus elegans* (E). Scale bars: 1 μm. Also shown are the corresponding two-dimensional profile plots representing spatial fluctuations in dark (keratin) and light (air) areas in the spongy layer and the coefficient of variation (CV) in the spacing between wave peaks (as an index of nanostructural regularity), in addition to the two-dimensional Fourier power spectra and associated spatial frequencies (*r*) given by the internal radius of the rings. F, G, also shown, for comparison, are TEM images of a cross-section of a feather barb collected from the black throat of a male *Malurus lamberti lamberti* (F) and the rufous shoulder of a male *Malurus amabilis* (G). Scale bars: 4 μm. Abbreviations: C, cortex; M, melanin granule; SL, spongy layer; V, vacuole.

to determine whether nanostructures are sufficiently organized at an appropriate scale to produce colour by coherent light scattering alone (Prum *et al.*, 1999; Shawkey *et al.*, 2003). For all images, the largest available square portion of keratin and air uninterrupted by melanin granules, cell boundaries or keratin cortex (280–1940 pixels^2) was selected (Fig. 3). We then created two-dimensional Fourier power spectra for each selected portion. All structurally coloured feather barbs showed discrete rings in the Fourier power spectra (Fig. 3B–E). For each ring, we took five measurements of the internal radius (in nanometres per cycle) to estimate the characteristic spatial frequency of the spongy layer (with small values of spatial frequency being associated with small scattering elements).

Nanostructural variation

Both the size and the regularity of the scattering elements in the spongy layer may affect aspects of the reflected colour (Shawkey *et al.*, 2003, 2005; D'Alba *et al.*, 2012). Therefore, for all structurally coloured patches, we measured the diameter of 15 keratin rods and 15 circular air spaces on each TEM image (Fig. 3B–E). The diameters of keratin rods and air spaces were not correlated ($|r| = 0.02$); therefore, we summed the average diameters of keratin rods and air spaces to obtain the distance between scatterers (Prum *et al.*, 2003; Shawkey *et al.*, 2005). In addition, we used ImageJ v.1.51 to produce profile plots of barb TEM images. We used the same selected square portions corresponding to entire areas of the spongy layers from the TEM images as above in the Fourier analysis. The profile plot shows a two-dimensional waveform, representing the spatial density fluctuation in the intensity of pixels (i.e. proxy for spatial variation in refractive index of keratin and air) within the selected area (Fig. 3B–E). Specifically, it displays a 'column average plot', where the x-axis in the waveform represents the horizontal distance through the selection and the y-axis the vertically averaged pixel intensity. We took 15 measurements of the distance between the peaks in the waveform and then calculated the coefficient of variation (CV) of the inter-peak distance as a measure of nanostructural regularity. This method has been used in previous studies investigating spatial regularity of spongy layer channels (D'Alba *et al.*, 2012).

Statistical analyses

All analyses were done in R v.3.4.0. Given that black and rufous feathers have little, degraded or no spongy layer, the analyses described below were performed on structurally coloured patches only. We used a meta-analytical approach to the study of variation (Hadfield & Nakagawa, 2010), which accounts for sampling error, multiple measurements per species and phylogenetic relatedness, implemented using the package 'MCMCglmm' (Hadfield, 2010).

First, to determine which morphological variables or combinations thereof represented independent axes of variation, we performed a principal component analysis (PCA) on the six morphological variables: (1) the thickness of the keratin cortex; (2) the thickness of the spongy layer; (3) the ratio of melanin to spongy layer; (4) the spatial frequency of the spongy layer provided by the Fourier analysis; (5) the distance between scatterers (calculated as the sum of the diameters of keratin rods and air spaces); and (6) the nanostructural regularity (for details, see Supporting Information, Appendix S3). Some of these variables are strongly intercorrelated, and PCA removed issues of collinearity between explanatory variables. The PCA indicated that the first four principal components, PC1–PC4, explain 88% of variation all together (see Supporting Information, Appendix S3 and Results).

We then tested whether these principal components are correlated with chromatic and achromatic variation. To do this, for each colorimetric variable, i.e. x, y, z (computed using either U- or V-type visual sensitivity functions) and perceived brightness, we fitted the colorimetric variable as the response variable and PC1–PC4 as (independent, uncorrelated) explanatory variables. Random effects included phylogenetic relatedness (as the inverse of the phylogenetic covariance matrix; Hadfield & Nakagawa, 2010; using the phylogeny of Marki *et al.*, 2017; Supporting Information, Fig. S1) and species identity, because in some species more than one plumage patch was measured. Sampling error variances (i.e. squared SE for each unique patch) for each chromatic coordinate or perceived brightness estimate were also included in the models to account for this uncertainty. We used a relatively uninformative inverse gamma prior for the residuals and Cauchy priors for random effects to improve model convergence when random effect variances are close to zero, and normal distributions centred on zero with large variances as fixed effects priors. We ran 101 000 iterations per model, from which we discarded the initial 1000 (burn-in period). Each chain was sampled at an interval of 100 iterations, meaning that the effective sample size was 1000.

Model convergence was assessed using trace graphs and autocorrelation plots. For each model, we computed marginal (fixed effects) and conditional (fixed + random effects) R^2 values (Nakagawa & Schielzeth, 2013). Chiefly, we computed total variance as the sum of the variances from fixed effects ('Sol' components in an MCMCglmm model), random effects and residual variance ('VCV' components in an MCMCglmm model, in this case species identity,

phylogenetic relatedness and residuals). Marginal R^2 values were obtained by dividing fixed effect variance by total variance, whereas conditional R^2 was obtained by dividing fixed effect variance plus random effect variance by total variance.

We then used the same Bayesian phylogenetic mixed model approach, fitting hue, UV chroma, spectral saturation or brightness as the response variable instead. We also analysed the separate effects of each of the six morphological variables on chromatic and achromatic variation by using the same Bayesian phylogenetic mixed model approach as above, i.e. fitting each colorimetric variable as the response variable, but with each morphological variable as a single explanatory variable (centred and scaled) in separate models. Data for all models can be found in the Supporting Information (Appendix S4).

Moreover, we assessed the degree of phylogenetic effects on each colorimetric and morphological variable, again using a Bayesian phylogenetic mixed model approach. We fitted each colorimetric or morphological variable as the response variable in separate models. In all models, we fitted a simple intercept as the explanatory variable, and the same random effects as above. We then determined the phylogenetic signal λ (i.e. the proportion of variation accounted for by phylogenetic relatedness relative to the total variation accounted by the random effects; Hadfield & Nakagawa, 2010).

RESULTS

Male nuptial plumage in fairy-wrens

Structurally coloured patches of the nuptial plumages of male fairy-wrens included various blue (light blue, azure, cobalt blue, navy blue, etc.) and indigo plumages, in addition to one case of purple plumage (in male *M. coronatus*; Figs 1, 2). Only the distal barbs of the feathers displayed the structural colour and had generally few or no barbules, whereas the proximal barbs displayed either a black (for blue and indigo feathers) or rufous (for purple feathers) coloration. In contrast, black and rufous feathers had both barbs and barbules, and rufous feathers also displayed a black coloration in their proximal part.

Reflectance spectrometry and avian visual model

Reflectance spectra of all blue and indigo patches were characterized by the presence of one or two discrete peaks in the UV and/or blue range (Fig. 2; Supporting Information, Fig. S2). The main peak was located between 360 and 540 nm, i.e. in most cases in the blue range, but in a few cases in the UV or green range (Fig. 2; Supporting Information, Fig. S2). In contrast, the second peak, when present, was always found between 325 and 375 nm, i.e. in the UV range, and in many cases it appeared as a 'shoulder' (i.e. not a distinct peak) or almost fully merged with the main peak (Fig. 2; Supporting Information, Fig. S2). In particular, spectra of very dark blue and indigo patches (i.e. the throat of *M. cyaneus*, *M. elegans* and *M. pulcherrimus*, and the rump of *M. cyanocephalus*) peaked in the UV range at a low reflectance value (< 15%; Fig. 2; Supporting Information, S2). Likewise, the reflectance spectrum of the purple crown of *M. coronatus* was characterized by two discrete peaks, the smaller one being in the UV range (at 340 nm) and the higher one in the blue range (at 460 nm); however, it also exhibited a steep increase between 550 and 700 nm, i.e. towards the red range, unlike other spectra (Fig. 2).

Plotting spectra in the bird visual space showed a relatively large colour span in the visual space of both U- and V-type species (Fig. 2; Supporting Information, Fig. S4). In this representation, the main axes of chromatic variation were z (range: U-type eyes, 11.5 jnd; V-type eyes, 11.1 jnd) and y (range: U-type eyes, 11.3 jnd; V-type eyes, 10.4 jnd), whereas variation along x was less marked (range: U-type eyes, 4.5 jnd; V-type eyes, 5.1 jnd). Achromatic variation was also high among the studied colours, with a range of 17.4 jnd.

Reflectance spectra of black and rufous patches displayed no discrete peaks; spectra measured on black patches were flat across the entire avian visual range (very low reflectance), whereas rufous spectra exhibited low reflectance between 300 and 525 nm, and a gradual and steep increase between 525 and 700 nm, i.e. towards the red range (Supporting Information, Fig. S3).

Feather structure

All 30 structurally coloured feather barbs we examined had an oval or round shape and were characterized by the presence of a medullary spongy layer located beneath a keratin cortex and on top of a layer of melanin granules surrounding large, hollow central vacuoles (Fig. 3A; Supporting Information, Appendix S2). The spongy layer was typically composed of a matrix of irregularly shaped keratin channels and air spaces (Fig. 3B–E), forming a 'quasi-ordered array' (Prum *et al.*, 2003). The dimensions of these various components showed substantial variation among the barbs examined (Table 1; Fig. 3). In particular, all feather barbs showed discrete rings in the Fourier power spectra (Fig. 3), indicating high levels of nanostructural uniformity and organization (Prum *et al.*, 1998, 1999) and allowing the production of colour by coherent light scattering alone.

In contrast, black and rufous feather barbs exhibited a pointed shape and were characterized by

Table 1. Dimensions of micro- and nanostructural components of feather barbs

Taxon	Plumage patch	Cortex thickness (nm)	SL thickness (nm)	Ratio of melanin/SL	SL spatial frequency (nm)	Diameter of keratin channels (nm)	Diameter of air spaces (nm)	SL irregularity
Malurus cyanocephalus bonapartii	Crown	4153.9 ± 480.8	11 305.9 ± 1964.0	0.09	242.2 ± 6.9	48.8 ± 2.1	128.3 ± 6.2	0.26
Malurus cyanocephalus bonapartii	Throat	2216.2 ± 450.3	2748.3 ± 350.2	0.10	184.4 ± 3.4	52.6 ± 2.5	110.5 ± 6.0	0.34
Malurus cyanocephalus bonapartii	Flank	2216.1 ± 750.2	3278.1 ± 684.8	0.14	194.5 ± 5.4	43.9 ± 2.2	105.7 ± 4.6	0.25
Malurus cyanocephalus bonapartii	Rump	4341.5 ± 1035.1	4152 ± 508.0	0.25	187.6 ± 4.9	60.1 ± 3.1	115.8 ± 6.4	0.30
Malurus cyanocephalus bonapartii	Shoulder	2601.8 ± 713.7	7079.9 ± 549.2	0.14	218.4 ± 4.7	57.3 ± 2.8	112.9 ± 4.4	0.28
Malurus coronatus coronatus	Crown	2873.2 ± 182.0	1603.8 ± 220.1	0.52	184.0 ± 5.3	86.9 ± 3.2	86.2 ± 2.6	0.26
Malurus elegans	Crown	2032.5 ± 522.3	4786.4 ± 642.6	0.15	263.9 ± 4.4	65.4 ± 4.2	170.5 ± 10.2	0.62
Malurus elegans	Cheek	2207.9 ± 258.1	5487.8 ± 655.1	0.11	230.2 ± 15.9	80.9 ± 3.9	121.7 ± 5.5	0.35
Malurus elegans	Throat	3094.3 ± 542.0	3021.8 ± 304.2	0.59	176.5 ± 3.1	59.2 ± 3.6	86.2 ± 6.1	0.25
Malurus pulcherrimus	Crown	1903 ± 185.6	5477.8 ± 514.2	0.11	167.0 ± 5.9	47.5 ± 1.4	96.9 ± 5.2	0.18
Malurus pulcherrimus	Cheek	4048.6 ± 570.8	8834.2 ± 928.4	0.03	182.3 ± 6.7	62.3 ± 2.7	132.6 ± 7.9	0.27
Malurus pulcherrimus	Throat	3221.9 ± 467.8	2748.3 ± 350.2	0.39	189.2 ± 0.9	60.0 ± 2.2	111.3 ± 4.8	0.20
Malurus amabilis	Crown	2668.5 ± 318.4	6086.6 ± 520.6	0.07	224.3 ± 3.0	68.2 ± 2.7	111.6 ± 5.2	0.42
Malurus amabilis	Cheek	2779.5 ± 704.2	12 269.7 ± 1550.1	0.02	220.2 ± 5.3	61.5 ± 2.6	121.0 ± 5.8	0.32
Malurus lamberti lamberti	Crown	2632.6 ± 452.2	7908.1 ± 671.3	0.13	189.8 ± 6.8	66.0 ± 4.1	136.9 ± 6.3	0.35
Malurus lamberti lamberti	Cheek	1408.1 ± 74.4	6834.7 ± 446.9	0.12	208.4 ± 2.2	59.4 ± 2.5	142.5 ± 6.8	0.42
Malurus lamberti assimilis	Crown	1605.4 ± 241.0	3250.2 ± 446.1	0.15	186.1 ± 2.7	63.6 ± 4.1	123.6 ± 7.2	0.31
Malurus lamberti assimilis	Cheek	3562.5 ± 905.4	5989.0 ± 526.6	0.03	239.4 ± 4.8	74.3 ± 4.6	168.7 ± 10.3	0.39
Malurus cyaneus cyaneus	Crown	1877.6 ± 116.1	8854.5 ± 1025.9	0.08	169.3 ± 6.4	71.1 ± 2.5	109.1 ± 4.0	0.25
Malurus cyaneus cyaneus	Cheek	1845.3 ± 172.6	8301.8 ± 1578.0	0.03	216.4 ± 2.7	74.9 ± 2.5	107.6 ± 2.4	0.18
Malurus cyaneus cyaneus	Throat	3393.1 ± 720.7	2611.8 ± 192.6	0.03	169.8 ± 2.5	58.4 ± 2.1	71.9 ± 2.4	0.20
Malurus splendens splendens	Crown	3654.6 ± 559.7	13 248.4 ± 653.3	0.03	161.2 ± 5.3	57.7 ± 3.0	107.6 ± 2.6	0.20

Table 1. Continued

Taxon	Plumage patch	Cortex thickness (nm)	SL thickness (nm)	Ratio of melanin/SL	SL spatial frequency (nm)	Diameter of keratin channels (nm)	Diameter of air spaces (nm)	SL irregularity
Malurus splendens splendens	Throat	1439.4 ± 140.0	4130.1 ± 486.4	0.42	189.1 ± 2.6	61.2 ± 2.6	121.9 ± 4.6	0.21
Malurus splendens melanotus	Crown	3031.1 ± 423.1	7277 ± 1405.2	0.12	214.9 ± 4.9	70.7 ± 2.0	120.2 ± 5.3	0.20
Malurus splendens melanotus	Cheek	1901.7 ± 159.4	11 230.0 ± 1885.3	0.01	208.5 ± 2.8	77.1 ± 3.2	128.8 ± 6.0	0.24
Malurus splendens melanotus	Throat	1600.5 ± 66.7	6172.9 ± 971.6	0.09	193.3 ± 1.9	64.7 ± 2.3	142.1 ± 4.7	0.22
Malurus splendens callainus	Crown	3052.9 ± 297.9	25 284.3 ± 2985.9	0.05	213.4 ± 2.3	56.4 ± 2.2	129.4 ± 4.8	0.33
Malurus splendens callainus	Cheek	868.7 ± 84.8	3149.8 ± 248.3	0.31	189.1 ± 8.4	66.7 ± 2.6	114.1 ± 4.8	0.38
Malurus splendens callainus	Throat	2399.6 ± 323.7	17 258.0 ± 2396.8	0.06	190.0 ± 1.9	56.6 ± 3.1	116.1 ± 5.1	0.26
Malurus leucopterus leuconotus	All*	1280.2 ± 211.6	2517.4 ± 259.7	0.27	226.2 ± 1.6	63.0 ± 2.1	151.4 ± 6.2	0.28

For each studied patch are shown the means (± SEM) of the cortex thickness, spongy layer (SL) thickness, SL spatial frequency (from Fourier analysis), diameter of keratin channels and diameter of circular air spaces, and the values of the ratio of melanin to SL (areas) and of SL irregularity.

the presence of numerous melanin granules within a thicker keratin cortex (mean ± SE = 3.04 ± 0.22 μm, vs. 2.53 ± 0.16 μm for structurally coloured barbs) surrounding little or no spongy layer (N = 3 black samples out of eight had no spongy layer, and all five rufous samples had extremely degraded spongy layers) and hollow central vacuoles (Fig. 3F, G). In particular, rufous barbs displayed a large amount of relatively small and round melanin granules, suggesting that they mainly contained phaeomelanin (Liu *et al.*, 2003). Additionally, when a spongy layer was present, it was notably degraded by holes (absence of keratin) and often interrupted by melanin granules (Fig. 3F, G).

Variation in feather structure and colour

We report results for colour variability as computed using U-type visual sensitivity functions; results using V-type functions were generally similar see Supporting Information (Tables S3–S12). Analyses were run with the main principal components provided by the PCA performed on the six morphological variables and for each morphological variable separately.

The PCA performed on the six morphological variables showed that 88% of morphological variation could be summarized by four principal components (Supporting Information, Appendix S3). Specifically, PC1 has negative loadings for the spatial frequency of the spongy layer, the distance between scatterers and the spongy layer irregularity (Supporting Information, Appendix S3), indicating that spongy layers of large spatial frequency also have more distant scattering elements and are more irregular. PC1 therefore represents the negative spatial frequency of the spongy layer. In contrast, PC2, PC3 and PC4 have a moderately to substantially strong loading for, respectively, the thickness of the spongy layer (positive), the thickness of the keratin cortex (positive) and the ratio of melanin to spongy layer (negative; Supporting Information, Appendix S3), indicating that each of these morphological variables tends to vary independently. Hence, PC2 mainly represents the thickness of the spongy layer, PC3 the thickness of the cortex and PC4 the negative ratio of melanin to spongy layer.

Variation along the x-axis (i.e. stimulation of the VS cone relative to the S cone) was affected by the spatial frequency of the spongy layer [PC1, marginal R^2 (U-/V-type) = 0.21/0.25; Fig. 4; Supporting Information, Tables S3 and S9]; reflectance spectra richer in shorter wavelengths were the result of spongy layers of lower spatial frequency. This correlation was confirmed by the analysis of the separate effects of each morphological variable (Tables S5 and S10).

Variation along the z-axis (i.e. stimulation of the L cone relative to VS + S + M cones) was predicted by the spatial frequency (PC1) and thickness (PC2) of the spongy layer and the thickness of the cortex [PC3, marginal R^2 (U-/V-type) = 0.63/0.65; Fig. 4; Supporting Information, Tables S3 and S9]. Feathers relatively poor in short- and middle-wavelength reflectance (UV–green) had barbs with a spongy layer of lower spatial frequency, a thinner spongy layer and/or a thicker cortex. In addition, analysis of the separate effects of each morphological variable indicated that such feathers also tend to have a spongy layer sitting above a relatively larger amount of melanin granules (Supporting Information, Tables S7 and S12; Fig. S6).

No morphological variable was correlated in a statistically significant manner with variation along the y-axis (i.e. stimulation of the M cone relative to VS + S cones; Fig. 4) based on the full model including PC1–PC4 [marginal R^2 (U-/V-type) = 0.28/0.26; Supporting Information, Tables S3 and S9]. However, analysis of the separate effects of each morphological variable indicated a possible influence of nanostructural regularity (when using U-type functions only; Supporting Information, Tables S6 and S11; Fig. S6). More irregular spongy layers tend to be associated with a higher stimulation of the M (green-sensitive) cone relative to the VS and S cones (UV and blue).

Achromatic variation (perceived brightness) was associated with the spatial frequency of the spongy layer (PC1) and the thickness of the cortex (PC3, marginal R^2 = 0.65; Fig. 4; Supporting Information, Table S3; Fig. S6). Barbs with a spongy layer of larger spatial frequency or a thinner cortex were brighter. Moreover, analysis of the separate effects of each morphological variable indicated that barbs with a thicker spongy layer or a spongy layer sitting above a relatively smaller amount of melanin granules also tend to be brighter (Supporting Information, Table S8; Fig. S6).

Additionally, results indicated that the spatial frequency of the spongy layer was positively correlated with hue (marginal R^2 = 0.46; Supporting Information, Table S4; Fig. S7) and negatively correlated with UV chroma (marginal R^2 = 0.20; Supporting Information, Table S4; Fig. S7). No morphological variable was correlated with spectral saturation (Supporting Information, Table S4). Brightness (average reflectance) was mainly correlated with the spatial frequency of the spongy layer (PC1; Supporting Information, Table S4; Fig. S7).

Finally, we assessed the degree of phylogenetic constraint on each colorimetric and morphological variable. Phylogenetic effects appeared relatively weak for all variables ($\lambda \leq 0.34$; Supporting Information, Table S13).

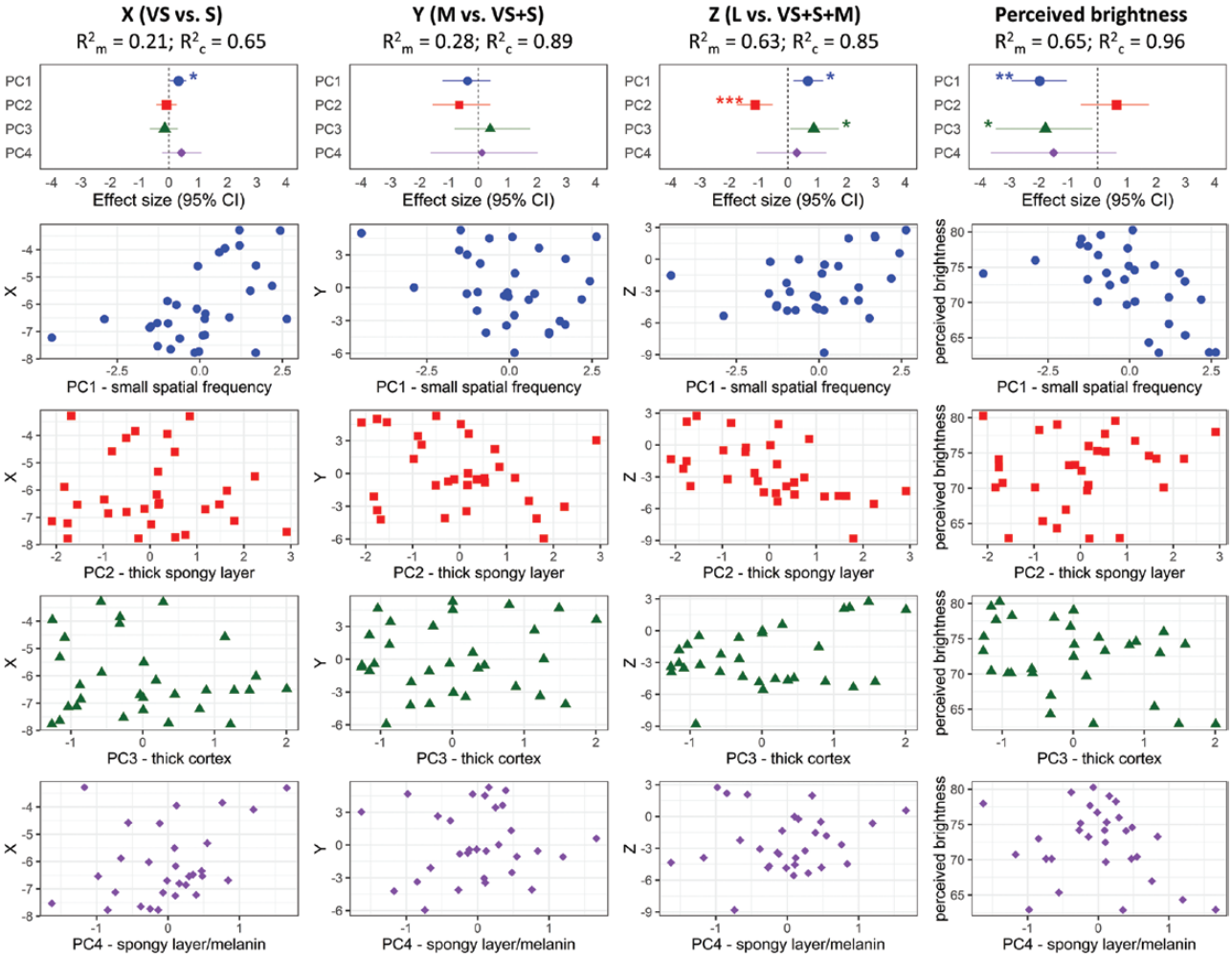

Figure 4. Chromatic and achromatic variation among structural colours in male fairy-wrens is related to different structural elements of feather barbs. The first row depicts the effect size estimates [posterior means and 95% credible intervals (CI); based on the full models presented in Supporting Information, Table S3] of principal component (PC)1, PC2, PC3 and PC4, on the response variables: chromatic coordinates (x, y and z, computed using U-type visual sensitivities) and perceived brightness (all N = 30). Rows below depict scatterplots between each PC and all response variables, where PCs are identified by colour and shape. Higher values of PC1 represent mainly smaller spatial frequencies of the spongy layer, higher values of PC2 a thicker spongy layer, higher values of PC3 a thicker cortex, and higher values of PC4 a higher relative amount of spongy layer compared with melanin. The x-coordinate represents stimulation of the VS cone relative to the S cone. Higher values of the y-coordinate represent higher stimulation of the M cone relative to VS and S cones. The z-coordinate represents higher relative stimulation of the L cone compared with the other three. Marginal and conditional R^2 values (R^2_m and R^2_c, respectively) are also presented. *P < 0.05, **P < 0.01, ***P < 0.001.

DISCUSSION

We show that differences in 30 patches of male structural plumage colours across nine species of fairy-wrens are caused by differences in the amount, dimensions and arrangement of many structural elements of feather barb. More specifically, we found that: (1) chromatic variation is primarily related to the spatial frequency and thickness of the spongy layer, the relative amounts of spongy layer and melanin, and the thickness of the cortex; and (2) achromatic variation is correlated with the spatial frequency of the spongy layer and the thickness of the cortex. Our results therefore indicate that many independent characteristics of feather microstructure, rather than a single mechanism, contribute to chromatic and achromatic variation in non-iridescent structural colours as perceived by birds (see summary in Fig. 5).

Male fairy-wrens display structural colours that vary widely, including UV, indigo, various blue and purple hues (Figs 1, 2; Supporting Information, Figs

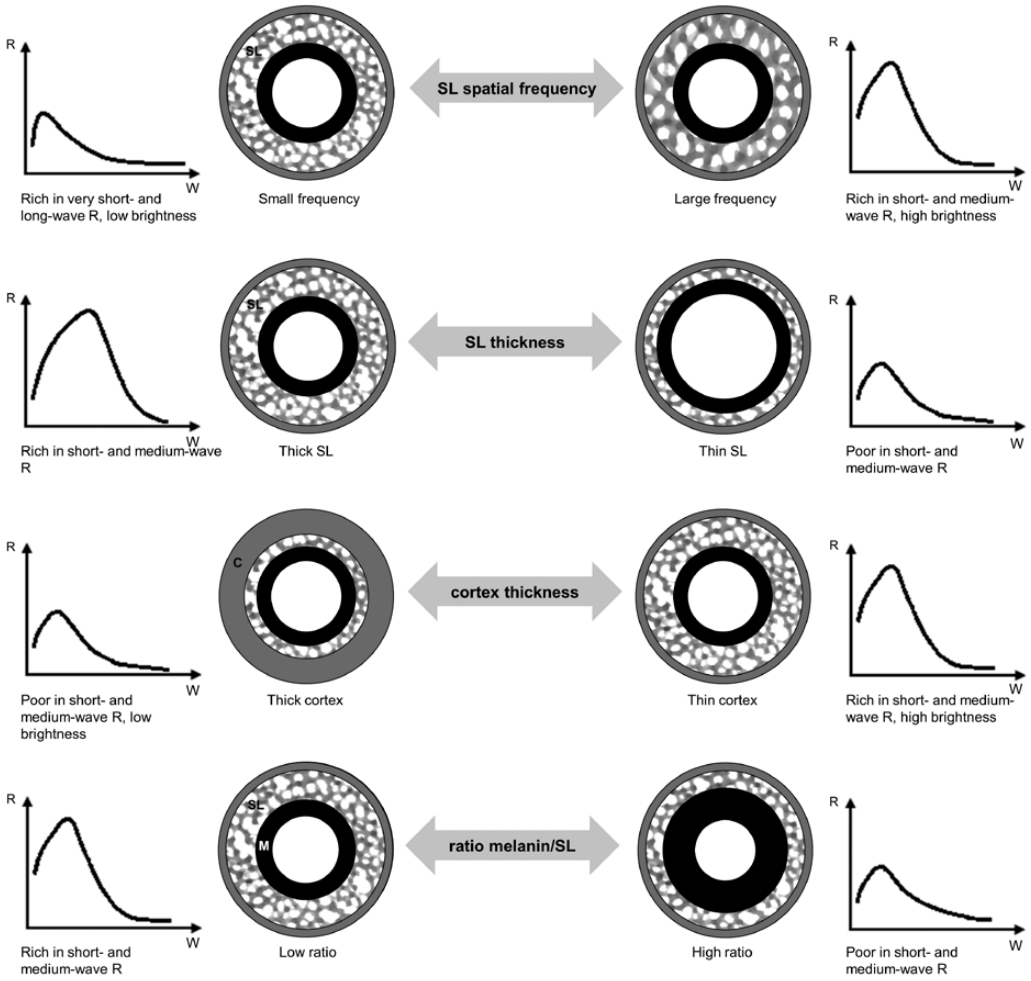

Figure 5. Schematic summary of the effects of multiple structural elements of feather barb on plumage reflectance. Barb morphology may affect plumage colour through changes in the spatial frequency and thickness of the spongy layer (SL), in the thickness of the cortex (C) and in the ratio of melanin (M) to spongy layer. For each depicted effect, the associated variation in the reflectance spectrum (R, reflectance; W, wavelength) is also schematized.

S2–S4). Transmission electron microscopy revealed that the barb microstructure of all sampled feathers is organized in a very similar way, with an outer keratin cortex above a medullary spongy layer, composed of a matrix of irregularly shaped keratin channels and air spaces, and a basal layer of melanin granules surrounding large, hollow central vacuoles (Fig. 3). This similarity suggests that the observed colour variation among the sampled feathers is not caused by the presence or absence of certain structural elements, but primarily by differences in the characteristics (size, density, etc.) of one or more of these elements. The discrete rings observed in the Fourier power spectra of all spongy layers showed that the colours are primarily produced by coherent light scattering owing to a nanostructural arrangement of keratin and air (uniform in all directions and highly ordered) in the feather barbs (Prum, 2006). This confirms the crucial role played by the medullary spongy layer in the production of structural colours (Shawkey *et al.*, 2003; Prum, 2006; D'Alba *et al.*, 2012; Saranathan *et al.*, 2012).

Variation in relative reflectance at short and medium wavelengths is generated by changes in the characteristics of the spongy layer. We found that lower spatial frequencies and smaller distances between scattering elements were responsible for reflectance spectra richer in shorter wavelengths (Fig. 4); tighter arrays of keratin and air are thus responsible for colours richer in UV. Additionally, we found some evidence, albeit limited, that more regular spongy layers tend to create colours that are richer in shorter wavelengths relative to medium wavelengths (Supporting Information, Fig. S6). As suggested by

Shawkey *et al.* (2003), increased uniformity in size of the scattering elements (i.e. increased regularity) is likely to result in a tighter grouping of the reflected light around the wavelength of peak reflectance (i.e. greater purity of the reflected colour), whereas increasing the variation in those elements might spread the reflected light over a broader spectrum, which in our case occurs mostly across the short- and medium-wavelength range. These observations agree with results presented by Saranathan *et al.* (2012), which show that across a large range of different structural colours (UV–red) the size and regularity of the scattering elements in the spongy layer predict the position of the reflectance peak and its saturation.

Variation in relative reflectance at long wavelengths is the result of changes in the spatial frequency and thickness of the spongy layer and the thickness of the cortex. Barbs comprising a spongy layer of lower spatial frequency, a thinner spongy layer and/or a thicker cortex generate colours richer in long-wavelength reflectance (corresponding to darker blue and purple feathers in our sample; Fig. 4). Given that the spongy layer is the main colour-producing element, responsible for the UV and blue hues, a decrease in its thickness will be associated with lower reflectance across the short-wavelength range. In addition, a decrease in the spatial frequency of the spongy layer or an increase in the thickness of the cortex generates darker blue colours. We also found some evidence that a spongy layer sitting on a relatively larger amount of melanin granules could account for colours richer in long-wavelength reflectance (Fig. 4; Supporting Information, Fig. S6). We speculate that this effect might be attributable to the fact that the light-absorption effect of melanin is going to be mostly evident across those wavelengths where coherent scattering by the spongy layer is reflecting light back (the short-wavelength range) rather than where reflectance is already low (in the long-wavelength range) and because melanin absorbs more strongly in shorter than in longer wavelengths (Xiao *et al.*, 2018).

The importance of melanin to structural colour production is also demonstrated by comparing structural colours with black and rufous colours. Both rufous and purple reflectance spectra exhibit a very similar gradual increase in the red range (Supporting Information, Figs S2, S3). This suggests that purple barbs (of the purple-crowned fairy-wren, *M. coronatus*) contain a basal layer consisting mainly of phaeomelanin, as previously proposed by Peters *et al.* (2013), and that phaeo- instead of eumelanin is primarily responsible for purple instead of blue plumage. Comparison of blue and black plumages confirms previous findings (Doucet *et al.*, 2004; Driskell *et al.*, 2010), in that most sampled black feather barbs (including those from *M. splendens*, *M. lamberti* and *M. coronatus*) contain a spongy layer that could produce a structural blue colour, but the degraded state of the spongy layer, in addition to a higher density of melanin and a thicker and more heavily melanized cortex, make them appear black. These vestiges of spongy layer suggest that evolutionary changes where melanin deposition obliterates structural colours might be common within this clade.

Feather perceived brightness (achromatic, dark-to-light variation) in our sample of structural colours was predicted by the spatial frequency of the spongy layer and the thickness of the keratin cortex, with spongy layers of larger spatial frequency and thinner cortices producing brighter feathers (Fig. 4; Supporting Information, Fig. S6). Previous studies of non-iridescent structural plumage colour suggested that the cortex acts primarily to absorb light (Finger, 1995; Shawkey *et al.*, 2005); hence, a thinner cortex will increase the amount of light reflected (total brightness). Moreover, thicker spongy layers and spongy layers sitting on relatively smaller amounts of melanin were also associated with brighter feathers (Supporting Information, Fig. S6). Both coherent (Benedek, 1971) and incoherent (Kerker *et al.*, 1966; Finger, 1995) scattering models of colour production predict positive associations between the number of scattering elements and brightness. In agreement with these theoretical predictions, for a given spatial frequency, a thicker spongy layer contains a larger number of scattering elements and, as a result, increases the amount of reflected light. In addition, previous research also proposed that the melanin density could affect brightness (Shawkey & Hill, 2006; but see Shawkey *et al.*, 2005); smaller amounts of melanin absorb less light, therefore causing more light to be reflected.

In conclusion, feather barb microstructure can vary in several independent ways to generate variation in plumage coloration: (1) in the thickness of the keratin cortex; (2) in various characteristics of the spongy layer, including its spatial frequency and thickness; or (3) in the relative amount of melanin sitting underneath the spongy layer (Fig. 5). Therefore, it is variation in many microstructural elements, rather than changes in a single key mechanism, that leads to the diversity of structural colours in the nuptial plumages of male fairy-wrens. The coexistence of several independent, evolutionarily labile (as shown by their low phylogenetic signal) parameters is likely to facilitate the evolution of a great variability of plumage colours.

Further studies should focus on how these different mechanisms mediate transitions between micro- and macro-evolutionary patterns. Specifically, are patterns of intraspecific colour variation (i.e. differences in coloration between individuals within a

population) generated by the same mechanisms that lead to differences in coloration between taxa? Or is intraspecific variation in colour restricted to certain mechanisms, whereas others are more likely to lead to the types of qualitative differences we expect between taxa? Understanding these processes will require a more sophisticated knowledge of the genetic and environmental factors behind variation in feather microstructure.

Whether the expression of structural colours is sensitive to environmental factors is debated (Prum, 2006) and empirical evidence mixed (Doucet, 2002; Johnsen *et al.*, 2003; Siefferman & Hill, 2005; Griggio *et al.*, 2009; Peters *et al.*, 2011). The spongy layer of structurally coloured feathers has been shown to develop through a self-assembly process that should be shielded largely from animal physiology, suggesting reduced scope for condition-dependent expression (Prum *et al.*, 2009; Parnell *et al.*, 2015). However, as we have shown here, the spongy layer itself is not the only determinant of colour variation, and other mechanisms could be affected by environmental variation and its effects on animal physiology. In contrast, some of the mechanisms identified here have been shown to be under strong genetic control (e.g. melanin deposition; Roulin & Ducrest, 2013). Our results suggest that, in the same way as fairy-wrens have become a model system in which to answer basic evolutionary questions from cooperative behaviour to sexual selection (Brouwer *et al.*, 2017; Medina *et al.*, 2017), they might also become a tractable model system in which to explore the mechanisms of colour evolution.

ACKNOWLEDGEMENTS

This research was approved by the Australian Bird and Bat Banding Scheme (license 2230); Western Australia Department of Parks and Wildlife; Australian Wildlife Conservancy; and the ethics committees of the School of Biological Sciences at Monash University. We thank the curators at Museum Victoria for access to specimen samples, A. McQueen, E. Enbody and J. A. Jones for feathers sampled from living birds and photographs, and the staff at Australian Wildlife Conservancy's Mornington Wildlife Sanctuary for their continued support and advice. We also thank C. Doutrelant, M. Webster and four anonymous reviewers for constructive feedback on the manuscript. We are grateful for support by the Australian Research Council (FT10100505 and DP150103595 to A.P.), the Society for the Study of Evolution (Rosemary Grant Research Award to M.F.), the Holsworth Wildlife Research Endowment–Equity Trustees Charitable Foundation (to M.F.) and the Australian Wildlife Conservancy and its supporters, the Flemish Research Funds (FWO G007117N) and the United States Air Force Office of Scientific Research (FA9550-1-18-0447) (both to M.D.S.).

REFERENCES

Andersson M. 1994. *Sexual selection*. Princeton: Princeton University Press.

Andersson S, Ornborg J, Andersson M. 1998. Ultraviolet sexual dimorphism and assortative mating in blue tits. *Proceedings of the Royal Society B: Biological Sciences* **265:** 445–450.

Benedek GB. 1971. Theory of transparency of the eye. *Applied Optics* **10:** 459–473.

Bitton PP, Janisse K, Doucet SM. 2017. Assessing sexual dicromatism: the importance of proper parameterization in tetrachromatic visual models. *PLoS ONE* **12:** e0169810.

Brouwer L, van de Pol M, Aranzamendi NH, Bain G, Baldassarre DT, Brooker LC, Brooker MG, Colombelli-Négrel D, Enbody E, Gielow K, Hall ML, Johnson AE, Karubian J, Kingma SA, Kleindorfer S, Louter M, Mulder RA, Peters A, Pruett-Jones S, Tarvin KA, Thrasher DJ, Varian-Ramos CW, Webster MS, Cockburn A. 2017. Multiple hypotheses explain variation in extra-pair paternity at different levels in a single bird family. *Molecular Ecology* **26:** 6717–6729.

Burkhardt D. 1989. UV vision: a bird's eye view of feathers. *Journal of Comparative Physiology. A, Sensory, Neural, and Behavioral Physiology* **164:** 787–796.

Cassey P, Ewen JG, Blackburn TM, Hauber ME, Vorobyev M, Marshall NJ. 2008. Eggshell colour does not predict measures of maternal investment in eggs of *Turdus* thrushes. *Die Naturwissenschaften* **95:** 713–721.

Cockburn A, Osmond HL, Double MC. 2008. Swingin' in the rain: condition dependence and sexual selection in a capricious world. *Proceedings of the Royal Society B: Biological Sciences* **275:** 605–612.

Cuthill IC. 2006. Color perception. In: Hill GE, McGraw K, eds. *Bird coloration.* Cambridge: Harvard University Press, 3–40.

D'Alba L, Kieffer L, Shawkey MD. 2012. Relative contributions of pigments and biophotonic nanostructures to natural color production: a case study in budgerigar (*Melopsittacus undulatus*) feathers. *The Journal of Experimental Biology* **215:** 1272–1277.

Darwin C. 1871. *The descent of man and selection in relation to sex*. London: John Murray.

Delhey K, Delhey V, Kempenaers B, Peters A. 2015. A practical framework to analyze variation in animal colors using visual models. *Behavioral Ecology* **26:** 367–375.

Delhey K, Hall M, Kingma SA, Peters A. 2013. Increased conspicuousness can explain the match between visual sensitivities and blue plumage colours in fairy-wrens. *Proceedings of the Royal Society B: Biological Sciences* **280:** 20121771.

Delhey K, Peters A. 2008. Quantifying variability of avian colours: are signalling traits more variable? *PLoS ONE* **3:** e1689.

Doucet SM. 2002. Structural plumage coloration, male body size, and condition in the blue-black grassquit. *Condor* **104:** 30–38.

Doucet SM, **Shawkey MD**, **Rathburn MK**, **Mays HL**, **Montgomerie R. 2004.** Concordant evolution of plumage colour, feather microstructure and a melanocortin receptor gene between mainland and island populations of a fairy-wren. *Proceedings of the Royal Society B: Biological Sciences* **271:** 1663–1670.

Driskell AC, **Prum RO**, **Pruett-Jones S. 2010.** The evolution of black plumage from blue in Australian fairy-wrens (Maluridae): genetic and structural evidence. *Journal of Avian Biology* **41:** 505–514.

Eliason CM, **Maia R**, **Shawkey MD. 2015.** Modular color evolution facilitated by a complex nanostructure in birds. *Evolution* **69:** 357–367.

Enbody ED, **Lantz SM**, **Karubian J. 2017.** Production of plumage ornaments among males and females of two closely related tropical passerine bird species. *Ecology and Evolution* **7:** 4024–4034.

Endler JA, **Mielke PWJ. 2005.** Comparing color patterns as birds see them. *Biological Journal of the Linnean Society* **86:** 405–431.

Fan M, **Teunissen N**, **Hall ML**, **Hidalgo Aranzamendi N**, **Kingma SA**, **Roast M**, **Delhey K**, **Peters A. 2018.** From ornament to armament or loss of function? Breeding plumage acquisition in a genetically monogamous bird. *The Journal of Animal Ecology* **87:** 1274–1285.

Finger E. 1995. Visible and UV coloration in birds: Mie scattering as the basis of color in many bird feathers. *Naturwissenschaften* **82:** 570–573.

Goldsmith TH. 1990. Optimization, constraint, and history in the evolution of eyes. *The Quarterly Review of Biology* **65:** 281–322.

Griggio M, **Serra L**, **Licheri D**, **Campomori C**, **Pilastro A. 2009.** Moult speed affects structural feather ornaments in the blue tit. *Journal of Evolutionary Biology* **22:** 782–792.

Hadfield J. 2010. MCMC methods for multi-response generalized linear mixed models: the MCMCglmm R package. *Journal of Statistical Software* **33:** 1–22.

Hadfield JD, **Nakagawa S. 2010.** General quantitative genetic methods for comparative biology: phylogenies, taxonomies and multi-trait models for continuous and categorical characters. *Journal of Evolutionary Biology* **23:** 494–508.

Hart NS. 2001. Variations in cone photoreceptor abundance and the visual ecology of birds. *Journal of Comparative Physiology. A, Sensory, Neural, and Behavioral Physiology* **187:** 685–697.

Hart NS, **Hunt DM. 2007.** Avian visual pigments: characteristics, spectral tuning, and evolution. *The American Naturalist* **169**(Suppl 1): S7–S26.

Hill GE, **McGraw K. 2006.** *Bird coloration*. Cambridge: Harvard University Press.

Johnsen A, **Delhey K**, **Andersson S**, **Kempenaers B. 2003.** Plumage colour in nestling blue tits: sexual dichromatism, condition dependence and genetic effects. *Proceedings of the Royal Society B: Biological Sciences* **270:** 1263–1270.

Kerker M, **Farone WA**, **Jacobsen RT. 1966.** Color effects in the scattering of white light by micron and submicron spheres. *Journal of the Optical Society of America* **56:** 1248–1255.

Liu Y, **Kempf VR**, **Brian Nofsinger J**, **Weinert EE**, **Rudnicki M, Wakamatsu K, Shosuke I, Simon JD. 2003.** Comparison of the structural and physical properties of human hair eumelanin following enzymatic or acid/base extraction. *Pigment Cell Research* **16:** 355–365.

Maia R, **Eliason C**, **Bitton P**, **Doucet SM**, **Shawkey MD. 2013.** pavo: an R package for the analysis, visualization and organization of spectral data. *Methods in Ecology and Evolution* **4:** 906–913.

Marki PZ, **Jønsson KA**, **Irestedt M**, **Nguyen JMT**, **Rahbek C**, **Fjeldså J. 2017.** Supermatrix phylogeny and biogeography of the Australasian Meliphagides radiation (Aves: Passeriformes). *Molecular Phylogenetics and Evolution* **107:** 516–529.

McGraw KJ. 2006. Mechanics of melanin coloration in birds. In Hill GE,McGraw KJ, eds. *Bird coloration. Vol. 1. Mechanisms and measurements*. Cambridge: Harvard University Press, 243–294.

Medina I, **Delhey K**, **Peters A**, **Cain KE**, **Hall ML**, **Mulder RA**, **Langmore NE. 2017.** Habitat structure is linked to the evolution of plumage colour in female, but not male, fairy-wrens. *BMC Evolutionary Biology* **17:** 35.

Nakagawa S, **Schielzeth H. 2013.** A general and simple method for obtaining R^2 from generalized linear mixed-effects models. *Methods in Ecology and Evolution* **4:** 133–142.

Odeen A, **Pruett-Jones S**, **Driskell AC**, **Armenta JK**, **Hastad O. 2012.** Multiple shifts between violet and ultraviolet vision in a family of passerine birds with associated changes in plumage coloration. *Proceedings of the Royal Society B: Biological Sciences* **279:** 1269–1276.

Olsson P, **Lind O**, **Kelber A. 2017.** Chromatic and achromatic vision: parameter choice and limitations for reliable model predictions. *Behavioral Ecology* **29:** 273–282.

Parnell AJ, **Washington AL**, **Mykhaylyk OO**, **Hill CJ**, **Bianco A**, **Burg SL**, **Dennison AJ**, **Snape M**, **Cadby AJ**, **Smith A**, **Prevost S**, **Whittaker DM**, **Jones RA**, **Fairclough JP**, **Parker AR. 2015.** Spatially modulated structural colour in bird feathers. *Scientific Reports* **5:** 18317.

Peters A, **Kingma SA**, **Delhey K. 2013.** Seasonal male plumage as a multi-component sexual signal: insights and opportunities. *Emu* **113:** 232–247.

Peters A, **Kurvers RH**, **Roberts ML**, **Delhey K. 2011.** No evidence for general condition-dependence of structural plumage colour in blue tits: an experiment. *Journal of Evolutionary Biology* **24:** 976–987.

Prum RO. 2006. Anatomy, physics, and evolution of structural colours. In: Hill GE, McGraw K, eds. *Bird coloration. Vol. 1. Mechanisms and measurements.* Cambridge: Harvard University Press, 295–353.

Prum RO, **Andersson S**, **Torres RH. 2003.** Coherent scattering of ultraviolet light by avian feather barbs. *Auk* **120:** 163–170.

Prum RO, **Dufresne ER**, **Quinn T**, **Waters K. 2009.** Development of colour-producing β-keratin nanostructures

in avian feather barbs. *Journal of the Royal Society, Interface* **6**(Suppl 2): S253–S265.

Prum RO, **Torres R**, **Williamson S**, **Dyck J. 1998.** Constructive interference of light by blue feather barbs. *Nature* **396:** 28–29.

Prum RO, **Torres R**, **Williamson S**, **Dyck J. 1999.** Two-dimensional Fourier analysis of the spongy medullary keratin of structurally coloured feather barbs. *Proceedings of the Royal Society B: Biological Sciences* **266:** 13–22.

R Development Core Team. **2014.** *R: a language and environment for statistical computing*. Vienna: R Foundation for Statistical Computing.

Roulin A, **Ducrest AL. 2013.** Genetics of colouration in birds. *Seminars in Cell & Developmental Biology* **24:** 594–608.

Saranathan V, **Forster JD**, **Noh H**, **Liew SF**, **Mochrie SG**, **Cao H**, **Dufresne ER**, **Prum RO. 2012.** Structure and optical function of amorphous photonic nanostructures from avian feather barbs: a comparative small angle X-ray scattering (SAXS) analysis of 230 bird species. *Journal of the Royal Society, Interface* **9:** 2563–2580.

Schneider CA, **Rasband WS**, **Eliceiri KW. 2012.** NIH Image to ImageJ: 25 years of image analysis. *Nature Methods* **9:** 671–675.

Shawkey MD, **Alba LD. 2017.** Interactions between colour-producing mechanisms and their effects on the integumentary colour palette. *Philosophical Transactions of the Royal Society B: Biological Sciences* **372:** 20160536.

Shawkey MD, **Estes AM**, **Siefferman LM**, **Hill GE. 2003.** Nanostructure predicts intraspecific variation in ultraviolet–blue plumage colour. *Proceedings of the Royal Society B: Biological Sciences* **270:** 1455–1460.

Shawkey MD, **Estes AM**, **Siefferman L**, **Hill GE. 2005.** The anatomical basis of sexual dichromatism in non-iridescent ultraviolet-blue structural coloration of feathers. *Biological Journal of the Linnean Society* **84:** 259–271.

Shawkey MD, **Hauber ME**, **Estep LK**, **Hill GE. 2006.** Evolutionary transitions and mechanisms of matte and iridescent plumage coloration in grackles and allies (Icteridae). *Journal of the Royal Society, Interface* **3:** 777–786.

Shawkey MD, **Hill GE. 2005.** Carotenoids need structural colours to shine. *Biology Letters* **1:** 121–124.

Shawkey MD, **Hill GE. 2006.** Significance of a basal melanin layer to production of non-iridescent structural plumage color: evidence from an amelanotic Steller's jay (*Cyanocitta stelleri*). *The Journal of Experimental Biology* **209:** 1245–1250.

Siddiqi A, **Cronin TW**, **Loew ER**, **Vorobyev M**, **Summers K. 2004.** Interspecific and intraspecific views of color signals in the strawberry poison frog *Dendrobates pumilio*. *The Journal of Experimental Biology* **207:** 2471–2485.

Siefferman L, **Hill GE. 2005.** Male eastern bluebirds trade future ornamentation for current reproductive investment. *Biology Letters* **1:** 208–211.

Stevens M, **Cuthill IC. 2007.** Hidden messages: are ultraviolet signals a special channel in avian communication? *BioScience* **57:** 501.

Vorobyev M, **Osorio D**, **Bennett AT**, **Marshall NJ**, **Cuthill IC. 1998.** Tetrachromacy, oil droplets and bird plumage colours. *Journal of Comparative Physiology. A, Sensory, Neural, and Behavioral Physiology* **183:** 621–633.

Xiao M, **Chen W**, **Li W**, **Zhao J**, **Hong Y**, **Nishiyama Y**, **Miyoshi T**, **Shawkey MD**, **Dhinojwala A. 2018.** Elucidation of the hierarchical structure of natural eumelanins. *Journal of the Royal Society, Interface* **15:** 20180045. https://doi.org/10.1098/rsif.2018.0045

SUPPORTING INFORMATION

Additional Supporting Information may be found in the online version of this article at the publisher's web-site:

Appendix S1. Feather sampling.

Appendix S2. Transmission electron microscopy images of feather barb morphology (zip file). Sample numbers match 'sample.number' variable in the Supporting Information (Appendix S4). Images can be found at: https://doi.org/10.6084/m9.figshare.8379014

Appendix S3. Principal components analysis (PCA).

Appendix S4. csv file with data used in analysis. Data can be found at: https://doi.org/10.6084/m9.figshare.8379014

Table S1. Feathers sampled from living birds (A) and specimens of male *Malurus* provided by Museum Victoria (B).

Table S2. Plumage patches of male *Malurus* measured using reflectance spectrometry. For *Malurus leucopterus leuconotus*, all blue patches (except the tail) were combined; for *Malurus melanocephalus*, all black patches were included. For *Malurus coronatus coronatus* and *Malurus cyaneus cyaneus*, both museum specimens and living birds were measured.

Table S3. Effects of morphological variation on chromatic (x, y and z) and achromatic (brightness) variation among structural colours in male fairy-wrens. Shown are the results of Bayesian phylogenetic mixed models examining the effects of principal component (PC)1, PC2, PC3 and PC4. Dependent variables were chromatic coordinates in the avian visual space (x, y and z) computed using U-type visual sensitivities, in addition to achromatic brightness (N = 30). Shown are posterior means for fixed effect coefficients and their 95% credible intervals (CI) and corresponding P-values ($^*P < 0.05$, $^{**}P < 0.01$ and $^{***}P < 0.001$; in bold), marginal (fixed effects) and conditional (fixed + random effects) R^2 values, and λ (phylogenetic signal).

Table S4. Effects of morphological variation on hue, ultraviolet chroma and spectral saturation among structural colours in male fairy-wrens. Shown are the results of Bayesian phylogenetic mixed models examining the effects of principal component (PC)1, PC2, PC3 and PC4, on hue, ultraviolet chroma and spectral saturation (N = 30).

Shown are posterior means for fixed effect coefficients and their 95% credible intervals (CI) and corresponding *P*-values (**P* < 0.05, ***P* < 0.01 and ****P* < 0.001; in bold), marginal (fixed effects) and conditional (fixed + random effects) R^2 values, and λ (phylogenetic signal).

Table S5. Separate effects of feather barb structural elements on the value of the *x*-coordinate. Shown are the results of Bayesian phylogenetic mixed models examining the separate effects (i.e. not accounting for other morphological variables) of cortex thickness, spongy layer (SL) thickness, ratio of melanin to SL, spatial frequency of the SL (from Fourier analysis), distance between scatterers (sum of the diameters of keratin channels and air spaces) and SL irregularity on the *x*-coordinate value of plumage structural colours of male *Malurus*, computed using U-type visual sensitivities (*N* = 30). Explanatory variables were centred and scaled. Shown are posterior means for fixed-effect coefficients and their 95% credible intervals (CI) and corresponding *P*-values (†*P* < 0.07, **P* < 0.05 and ****P* < 0.001; in bold), marginal (fixed effects) and conditional (fixed + random effects) R^2 values, and λ (phylogenetic signal).

Table S6. Separate effects of feather barb structural elements on the value of the *y*-coordinate. Shown are the results of Bayesian phylogenetic mixed models examining the separate effects (i.e. not accounting for other morphological variables) of cortex thickness, spongy layer (SL) thickness, ratio of melanin to SL, spatial frequency of the SL (from Fourier analysis), distance between scatterers (sum of the diameters of keratin channels and air spaces) and SL irregularity on the *y*-coordinate value of plumage structural colours of male *Malurus*, computed using U-type visual sensitivities (*N* = 30). Explanatory variables were centred and scaled. Shown are posterior means for fixed effect coefficients and their 95% credible intervals (CI) and corresponding *P*-values (**P* < 0.05; in bold), marginal (fixed effects) and conditional (fixed + random effects) R^2 values, and λ (phylogenetic signal).

Table S7. Separate effects of feather barb structural elements on the value of the *z*-coordinate. Shown are the results of Bayesian phylogenetic mixed models examining the separate effects (i.e. not accounting for other morphological variables) of cortex thickness, spongy layer (SL) thickness, ratio of melanin to SL, spatial frequency of the SL (from Fourier analysis), distance between scatterers (sum of the diameters of keratin channels and air spaces) and SL irregularity on the *z*-coordinate value of plumage structural colours of male *Malurus*, computed using U-type visual sensitivities (*N* = 30). Explanatory variables were centred and scaled. Shown are posterior means for fixed effect coefficients and their 95% credible intervals (CI) and corresponding *P*-values (**P* < 0.05, ***P* < 0.01 and ****P* < 0.001; in bold), marginal (fixed effects) and conditional (fixed + random effects) R^2 values, and λ (phylogenetic signal).

Table S8. Separate effects of feather barb structural elements on perceived brightness. Shown are the results of Bayesian phylogenetic mixed models examining the separate effects (i.e. not accounting for other morphological variables) of cortex thickness, spongy layer (SL) thickness, ratio of melanin to SL, spatial frequency of the SL (from Fourier analysis), distance between scatterers (sum of the diameters of keratin channels and air spaces) and SL irregularity on the brightness of plumage structural colours of male *Malurus* (*N* = 30). Explanatory variables were centred and scaled. Shown are posterior means for fixed effect coefficients and their 95% credible intervals (CI) and corresponding *P*-values (**P* < 0.05, ***P* < 0.01 and ****P* < 0.001; in bold), marginal (fixed effects) and conditional (fixed + random effects) R^2 values, and λ (phylogenetic signal).

Table S9. Effects of morphological variation on chromatic (*x*, *y* and *z*) variation among structural colours in male fairy-wrens. Shown are the results of Bayesian phylogenetic mixed models examining the effects of principal component (PC)1, PC2, PC3 and PC4. Dependent variables were chromatic coordinates in the avian visual space (*x*, *y* and *z*) computed using V-type visual sensitivities (*N* = 30). Shown are posterior means for fixed effect coefficients and their 95% credible intervals (CI) and corresponding *P*-values (†*P* < 0.07, **P* < 0.05 and ****P* < 0.001; in bold), marginal (fixed effects) and conditional (fixed + random effects) R^2 values, and λ (phylogenetic signal).

Table S10. Separate effects of feather barb structural elements on the value of the *x*-coordinate. Shown are the results of Bayesian phylogenetic mixed models examining the separate effects (i.e. not accounting for other morphological variables) of cortex thickness, spongy layer (SL) thickness, ratio of melanin to SL, spatial frequency of the SL (from Fourier analysis), distance between scatterers (sum of the diameters of keratin channels and air spaces) and SL irregularity on the *x*-coordinate value of plumage structural colours of male *Malurus*, computed using V-type visual sensitivities (*N* = 30). Explanatory variables were centred and scaled. Shown are posterior means for fixed effect coefficients and their 95% credible intervals (CI) and corresponding *P*-values (†*P* < 0.07 and **P* < 0.05; in bold), marginal (fixed effects) and conditional (fixed + random effects) R^2 values, and λ (phylogenetic signal).

Table S11. Separate effects of feather barb structural elements on the value of the *y*-coordinate. Shown are the results of Bayesian phylogenetic mixed models examining the separate effects (i.e. not accounting for other morphological variables) of cortex thickness, spongy layer (SL) thickness, ratio of melanin to SL, spatial frequency of the SL (from Fourier analysis), distance between scatterers (sum of the diameters of keratin channels and air spaces) and SL irregularity on the *y*-coordinate value of plumage structural colours of male *Malurus*, computed

using V-type visual sensitivities (N = 30). Explanatory variables were centred and scaled. Shown are posterior means for fixed effect coefficients and their 95% credible intervals (CI) and corresponding P-values, marginal (fixed effects) and conditional (fixed + random effects) R^2 values, and λ (phylogenetic signal).

Table S12. Separate effects of feather barb structural elements on the value of the z-coordinate. Shown are the results of Bayesian phylogenetic mixed models examining the separate effects (i.e. not accounting for other morphological variables) of cortex thickness, spongy layer (SL) thickness, ratio of melanin to SL, spatial frequency of the SL (from Fourier analysis), distance between scatterers (sum of the diameters of keratin channels and air spaces) and SL irregularity on the z-coordinate value of plumage structural colours of male *Malurus*, computed using V-type visual sensitivities (N = 30). Explanatory variables were centred and scaled. Shown are posterior means for fixed effect coefficients and their 95% credible intervals (CI) and corresponding P-values (†$P < 0.07$, *$P < 0.05$, **$P < 0.01$ and ***$P < 0.001$; in bold), marginal (fixed effects) and conditional (fixed + random effects) R^2 values, and λ (phylogenetic signal).

Table S13. Phylogenetic effects on feather colour and morphological variables. Shown are the results of Bayesian phylogenetic mixed models examining the degree of phylogenetic constraint on the x-, y- and z-coordinates computed using U- and V-type visual sensitivities and brightness (A) and on cortex thickness, spongy layer (SL) thickness, ratio of melanin to SL, spatial frequency of the SL (from Fourier analysis), distance between scatterers (sum of the diameters of keratin channels and air spaces) and SL irregularity (B) (N = 30). Shown are posterior means for λ (phylogenetic signal) and the 95% credible intervals.

Figure S1. **Phylogeny for the studied *Malurus* species based on the supermatrix phylogeny of** Marki *et al.* (2017). Patches sampled for barb morphology are indicated (blue represents structural colours, black eumelanin black feathers and red phaeomelanin-based rufous feathers).

Figure S2. Average (smoothed) reflectance spectra of plumage patches of male *Malurus*. Line colours correspond approximately to the feather colour perceived by the human eye. Sample sizes for each plumage patch are provided in the Supporting Information (Table S2). Taxon abbreviations: *ama.*, *Malurus amabilis*; *cor.*, *Malurus coronatus* (*coronatus*); *cya.*, *Malurus cyaneus* (*cyaneus*); *cyano.*, *Malurus cyanocephalus* (*bonapartii*); *ele.*, *Malurus elegans*; *lam. ass.*, *Malurus lamberti assimilis*; *lam. lam.*, *Malurus lamberti lamberti*; *leu.*, *Malurus leucopterus* (*leuconotus*); *pul.*, *Malurus pulcherrimus*; *spl. cal.*, *Malurus splendens callainus*; *spl. mel.*, *Malurus splendens melanotus*; *spl. spl.*, *Malurus splendens splendens*. Plumage patch abbreviations: all, the whole body except the wings and tail for *M. leucopterus*; ch, cheek; cr, crown; fl, flank; ru, rump; sh, shoulder; th, throat.

Figure S3. Average (smoothed) reflectance spectra of black and rufous plumage patches of male *Malurus*: A, head of *Malurus alboscapulatus moretoni*; and B, shoulder of *Malurus amabilis*. Line colours correspond approximately to the feather colour perceived by the human eye. Sample sizes for each plumage patch are provided in the Supporting Information (Table S2).

Figure S4. Average positions of the studied colour patches in the visual space of V-type species. The x-axis represents stimulation of the VS cone relative to the S cone. Higher values on the y-axis represent higher stimulation of the M cone relative to VS and S cones. The z-axis represents higher relative stimulation of the L cone compared with the other three [units are the just-noticeable difference (jnd)]. Taxon abbreviations: *ama.*, *Malurus amabilis*; *cor.*, *Malurus coronatus* (*coronatus*); *cya.*, *Malurus cyaneus* (*cyaneus*); *cyano.*, *Malurus cyanocephalus* (*bonapartii*); *ele.*, *Malurus elegans*; *lam. ass.*, *Malurus lamberti assimilis*; *lam. lam.*, *Malurus lamberti lamberti*; *leu.*, *Malurus leucopterus* (*leuconotus*); *pul.*, *Malurus pulcherrimus*; *spl. cal.*, *Malurus splendens callainus*; *spl. mel.*, *Malurus splendens melanotus*; *spl. spl.*, *Malurus splendens splendens*. Plumage patch abbreviations: all*, the whole body except the wings and tail for *M. leucopterus*; ch, cheek; cr, crown; fl, flank; ru, rump; sh, shoulder; th, throat. Sphere colours correspond approximately to the feather colour perceived by the human eye.

Figure S5. Influence of barbules on feather colour in the studied plumages. Shown are examples of (normalized and smoothed) reflectance spectra measured on the whole plumage patch (continuous line) and on a single barb (dotted line): A, throat of male *Malurus cyaneus cyaneus*; B, throat of male *Malurus pulcherrimus*; and C, flank of male *Malurus cyanocephalus bonapartii* (all three plumage patches are formed by feathers comprising barbules).

Figure S6. Scatterplots depicting the correlations between chromatic coordinates (x, y and z, computed using U-type visual sensitivities), perceived brightness and six components of barb morphological variation.

Figure S7. Scatterplots depicting the correlations between colorimetric variables (hue, saturation, ultraviolet chroma and brightness) and the first four principal components (PCs) summarizing variation in six components of barb morphology.

SHARED DATA

https://doi.org/10.6084/m9.figshare.8379014.